# PROCEEDINGS OF SPIE

SPIEDigitalLibrary.org/conference-proceedings-of-spie

# Electrical and optical properties of nickel-doped Ge2Sb2Te5 films produced by magnetron co-sputtering

Pengfei Guo, Gary A. Sevison, Joshua A. Burrow, Imad Agha, Andrew Sarangan

Pengfei Guo, Gary A. Sevison, Joshua A. Burrow, Imad Agha, Andrew Sarangan, "Electrical and optical properties of nickel-doped Ge2Sb2Te5 films produced by magnetron co-sputtering," Proc. SPIE 10730, Nanoengineering: Fabrication, Properties, Optics, and Devices XV, 107300L (19 September 2018); doi: 10.1117/12.2320843



Event: SPIE Nanoscience + Engineering, 2018, San Diego, California, United States

# Electrical and optical properties of nickel-doped Ge<sub>2</sub>Sb<sub>2</sub>Te<sub>5</sub> films produced by magnetron co-sputtering

Pengfei Guo<sup>1</sup>, Gary A. Sevison<sup>1</sup>, Joshua A. Burrow<sup>1</sup>, Imad Agha<sup>1,2</sup>, and Andrew Sarangan<sup>1</sup>

<sup>1</sup>Electro-Optics and Photonics Department, University of Dayton, Dayton, OH 45469, USA <sup>2</sup>Physics Department, University of Dayton, Dayton, OH 45469, USA

#### ABSTRACT

A magnetron co-sputtering system was used for producing nickel-doped Ge<sub>2</sub>Sb<sub>2</sub>Te<sub>5</sub> (GST-Ni) thin films. The nickel content in the thin film was adjusted by the ratio of the plasma discharge power applied to the GST and nickel targets, as well as a physical shuttering technique to further control the nickel deposition rate. The doping concentration of the film was confirmed using Energy Dispersion Spectroscopy (EDS) technique. Results from a four-point probe measurement indicate that the nickel doping can reduce the resistivity of GST in the amorphous state by nearly three orders of magnitude. The dopant's influence on crystallization behavior was studied by analyzing X-Ray Diffraction (XRD) patterns of the pure GST and GST-Ni at different annealing temperatures. To examine the structural changes due to the nickel dopant, the thin films were investigated with the aid of Raman scattering. Additionally, we extracted the optical constants for both the amorphous and crystalline states of undoped-GST and GST-Ni films by ellipsometry. The results indicate that at low doping concentrations nickel does not appreciably affect the optical constants, but dramatically improves the electrical conductivity. Therefore, nickel-doping of GST a viable method for designing optical devices for lower operating voltages at higher switching speeds.

**Keywords:** Phase change material, co-sputtering, Ge<sub>2</sub>Sb<sub>2</sub>Te<sub>5</sub>, nickel, doping, resistivity, Raman, refractive index, extinction coefficient.

#### 1. INTRODUCTION

Phase change materials (PCM) undergo a reversible structural change between crystalline and amorphous phases due to the application of heat, typically from an electrical source or optical source. Due to the vastly different optical and electrical properties between the two states, these materials can be used in devices with an internal nonvolatile memory state that can be switched. Among various materials, the pseudo-binary chalcogenide GeTe-Sb<sub>2</sub>Te<sub>3</sub>, particularly Ge<sub>2</sub>Sb<sub>2</sub>Te<sub>5</sub> (GST) has been the most widely studied material because of its fast crystallization speed, reversible phase transition and stability over a wide temperature range. Compared to other phase change materials such as VO<sub>2</sub>, which undergoes a volatile semiconductor to metal transition, GST is characterized by a large change in the real part of the refractive index while the imaginary part remains relatively small in both states. This property makes the GST suitable for components such as switchable phase retarders and form birefringence devices.<sup>1,2</sup>

However, GST has a large resistivity in its amorphous state of several hundred  $\Omega \cdot m$ . The crystalline phase has a much lower resistivity, by several orders of magnitude. This large difference in resistivity limits its use in high speed electronic devices because both states cannot be simultaneously impedance matched in a circuit. Additionally, the large resistivity of the amorphous state also requires a very high voltage to dissipate sufficient power in the film to induce the transition. Therefore, to enable faster switching, it is important to reduce the difference in resistivity between the amorphous and crystalline phases, but without significantly compromising their optical characteristics. In the past few years, a variety of dopant elements have been studied to modify the electrical properties of GST, such as nitrogen, a carbon, a varyen, silicon, aluminum, silver, titanium, nickel and copper.

Further author information: (Send correspondence to Pengfei Guo) Pengfei Guo: E-mail: guop01@udayton.edu, Telephone: 1 775 688 9615

Nanoengineering: Fabrication, Properties, Optics, and Devices XV, edited by Balaji Panchapakesan, Anne E. Sakdinawat, André-Jean Attias, Elizabeth A. Dobisz, Proc. of SPIE Vol. 10730, 107300L © 2018 SPIE · CCC code: 0277-786X/18/\$18 · doi: 10.1117/12.2320843

of the GST-based devices, none of them have shown the capability to reduce the resistivity of the amorphous state. Zhu et. al.<sup>11</sup> performed a doping regime by introducing nickel into the GST material to realize a smaller resistivity at amorphous state, which opened a way to switch the device to crystalline state with a smaller voltage. In this letter, beside showing the resistivity study on GST doped with nickel, the X-ray diffraction (XRD) analysis on the lattice structure between amorphous state to face-centered cubic (fcc) and hexagonal close packed (hcp) state were examined. The local structural information were studied by fitting the Raman spectra into seven Gaussian oscillators. To examine if there is a large change in optical property by doping, the refractive index and extinction coefficient of GST and GST-Ni at both amorphous and crystalline states were extracted by ellipsometry.

#### 2. FABRICATION PROCESS

The doped  $Ge_2Sb_2Te_5$  films were fabricated by magnetron co-sputtering. One of the cathode with the GST target was excited by a 13.56 MHz RF power supply and the other cathode with the nickel target was excited from a DC plasma generator. Prior to the deposition, Acetone-Methanol-Isopropyl alcohol (AMI) cleaning process is used to remove any organic contaminations from the substrate. They were then placed in the chamber and pumped down to a base pressure of 1  $\mu$ Torr to remove background gases. The RF power to the GST target was maintained at 100 W while the DC power to the nickel target was varied between 300 W to 15 W to control the amount of nickel content in the co-sputtered films. In order to obtain a sufficiently low nickel concentration, the power was reduced down to 15 W on the nickel target. However, at this very low power levels the plasma becomes unstable, resulting in poor run-to-run repeatability. Therefore, we employed a physical shuttering technique in company with 75 W DC power to further reduce the deposition rate of nickel without significantly reducing the plasma discharge power. This allowed us to achieve doping concentrations of 2% reliably and repeatably. After deposition, the film thicknesses were verified by measuring the step height using a stylus profiler.

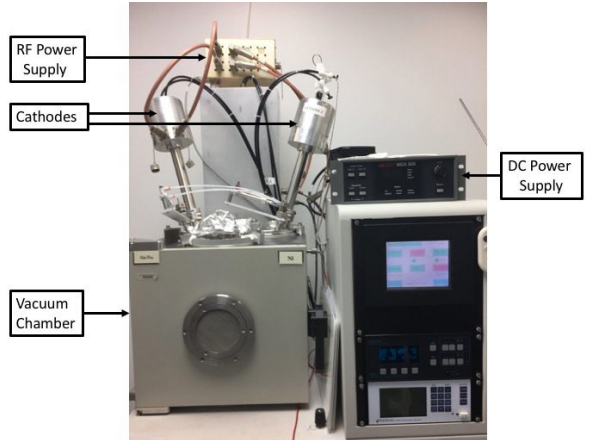


Figure 1: Magnetron co-sputter deposition system.

#### 3. RESULTS AND DISCUSSION

### 3.1 Composition analysis

The composition of the co-sputtered GST and GST-Ni films were examined by Energy Dispersion Spectroscopy (EDS). The results are shown in Figure 2. The physical shutter can greatly reduce the dopant concentration in the co-sputtered thin films. Compared to the GST films fabricated with thermal evaporation, <sup>13</sup> sputtering provides better films as the bottom part of the evaporated films could be enriched with more volatile species. Therefore, for GST thin film devices, sputtering is a preferred technique since it can provide a more uniform and condensed film.

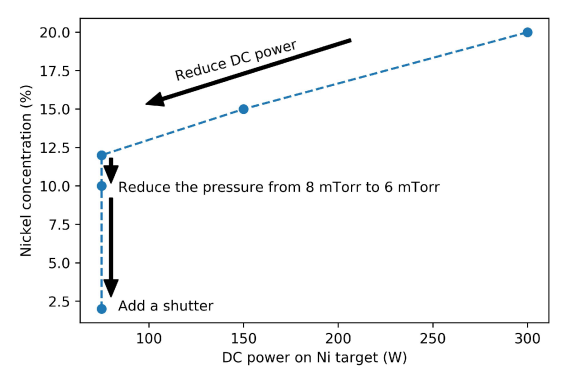


Figure 2: The variation of nickel concentration in the films at different experimental conditions.

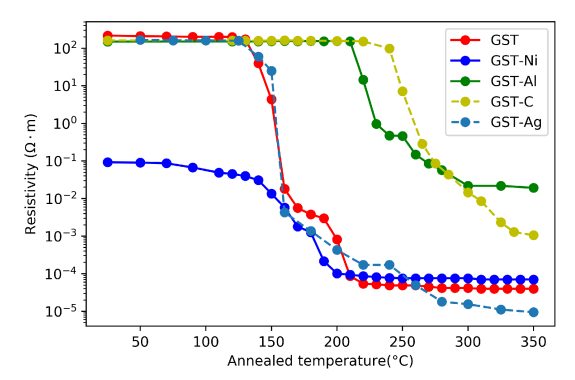


Figure 3: Resistivity as a function of annealed temperature for thin films of as-deposited pure GST, GST-Ni, GST-Al, GST-C, and GST-Ag.

#### 3.2 Resistivity analysis

The sheet resistance as a function of anneal temperature between 25 °C and 350 °C was measured for GST, GST-Ni, GST-Al, GST-C, and GST-Ag films using a custom-made four-point probe. By separating the current and voltage electrodes, the four-point probe can eliminate the contact resistance between the probe and the film during the measurement. Before each sheet resistance measurement, the samples were placed on a hot plate for 3 minutes to ensure an evenly distributed temperature on the film. After cooling down to room temperature, the sheet resistance of each film was measured. The measured resistivity of all films are summarized in Figure 3. All films show a higher resistivity in the amorphous state than the crystalline states. The undoped GST film shows two transitions, one from the amorphous state to the fcc state at 150 °C, and a less pronounced transition from the fcc state to the hcp state at 210 °C. The transition temperature from the amorphous to the fcc state agrees well with prior literature. Pepending on the doping species, a phase transition that is accompanied by a more or less a sharp drop in resistivity curve occurs at a different crystallization temperature  $T_c$ . It was found that nickel dopant can greatly reduce the resistivity of the amorphous state by three orders of magnitude which a significantly simpler impedance matching and lower switching voltages in device applications.

# 3.3 X-Ray Diffraction Analysis

X-Ray Diffraction (XRD) measurements were carried out to investigate the influence of the nickel doping on the crystallinity of GST films. The XRD patterns for GST and GST-Ni at different states are shown in Figure 4. There are no sharp peaks for the as-deposited GST and GST-Ni films in Figure 4 (a), which confirms the amorphous nature of these films. In both Figs 4 (b) and (c), the diffraction peaks of both samples are well aligned, which demonstrates that the small amount of nickel dopant does not significantly affect the crystalline structure of the GST film. A lower intensity of the XRD peaks in GST-Ni indicates a lower crystallinity in the

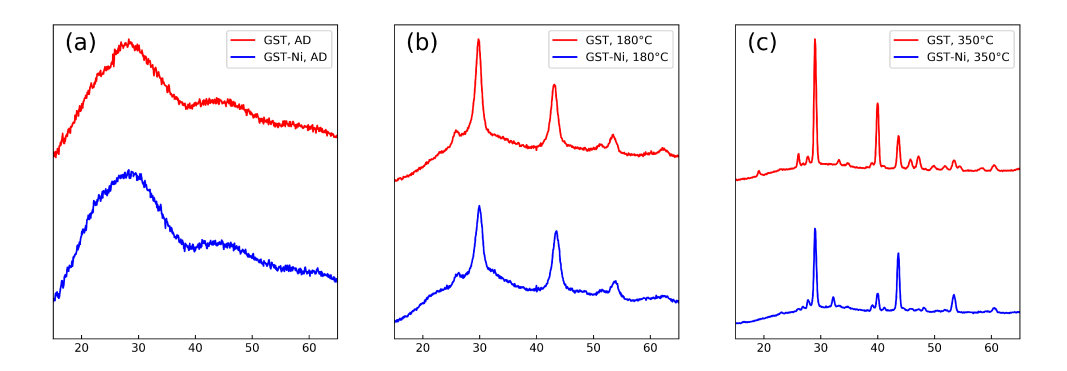


Figure 4: XRD patterns of the GST and Ni-GST films when (a) as-deposited , (b) after annealed at  $180\,^{\circ}$ C, and (c) after annealed at  $350\,^{\circ}$ C.

hcp state compared to pure GST. Since higher atomic alignment in the crystalline state can provide a higher electrical conductivity, the lower crystallinity may explain the slightly smaller electrical conductivity of GST-Ni in the crystalline state compared to the undoped GST.

## 3.4 Raman Analysis

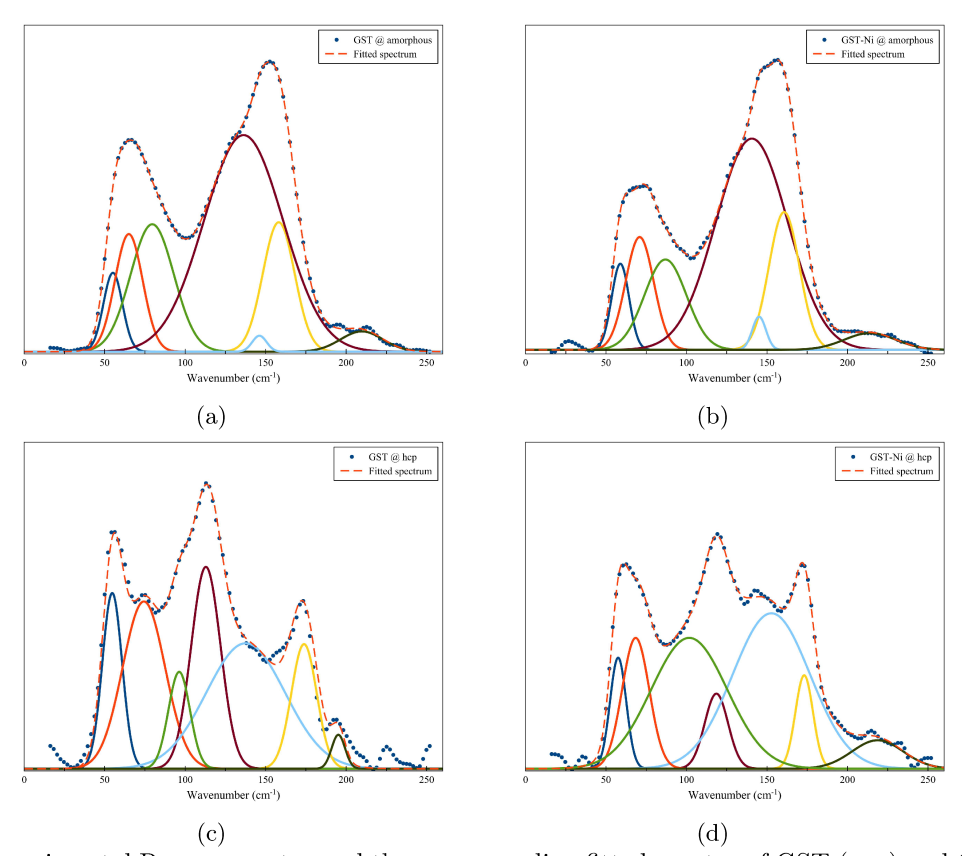


Figure 5: The experimental Raman spectra and the corresponding fitted spectra of GST (a, c) and GST-Ni films (b, d)

Table 1: The assignments of phonon modes in GST material fitted using seven Gaussian oscillators in the spectra.

	Peak position $(cm^{-1})$							
Amorphous	GST	55	65	80	136	146	158	209
	GST-Ni	59	71	87	141	145	161	214
Crystalline	GST	55	72	94	113	142	173	195
	GST-Ni	58	68	102	119	153	174	218

We used Raman spectroscopy to characterize the local structure of GST and GST-Ni, such as substitution and distortion. Figure 5 shows the fitted Raman spectra for the GST and GST-Ni films at both the amorphous state and crystalline state. The Gaussian oscillator model was used to study the vibrational modes in the GST systems by decomposing the experimental data into seven Gaussian oscillators. The peak positions of the Gaussian oscillators were summarized in the Table 1. The modes in Raman spectra of GST at amorphous state can be attributed to defective octahedra,  $GeTe_{4-n}Ge_n$  (n = 0, 1, 2) edge and/or corner-sharing tetrahedra and SbTe<sub>3</sub> pyramidal units. The modes of GST at crystalline state can be assigned to defective octahedra, cornersharing  $GeTe_{4-n}Ge_n$  (n = 0, 1, 2) and hexagonal  $Sb_2Te_3$ . The Raman spectra of both amorphous GST and GST-Ni have a typical two-humped shape in region 100 - 170 cm<sup>-1</sup>, in another words, 120 cm<sup>-1</sup> and 150 cm<sup>-1</sup>. These two frequencies are very close to the reported.<sup>17</sup> The peaks at around 60 and 80 is related with the bending modes  $v_4(F_2)$  and  $v_2(E)$  of the tetrahedra, respectively. 15, 18 The typical symmetric stretching mode  $(A_1)$  of corner-sharing tetrahedral units  $GeTe_{4-n}Ge_n$  (n=0,1,2) is around 120  $cm^{-1}$ . 15, 17–19 Around 150 to 160  $cm^{-1}$  is the edge-sharing tetrahedra in a-GeTe or the stretching modes of the  $Sb_2Te_3$  units. <sup>15,18,19</sup> The  $v_3(F_2)$ antisymmetric stretching mode is around 220 cm $^{-1}$ . Furthermore, based on the decomposing Gaussian curves summarized in Table 1, there is no dramatically difference between GST and GST-Ni at amorphous state and crystalline state, respectively, it indicates that there is no dramatic change took to the GST matrix by nickel doping. However, comparing to pure GST material, the Raman peaks of GST-Ni generally moves to a larger wavenumber, which may due to the substitution of Te atoms by Ni atoms in the structural units, since Te atoms are heavier than Ni atoms. The Te atoms can also be substituted by heavier atoms, such as W atoms, which induces blue shift in Raman peaks.<sup>15</sup>

## 3.5 Ellipsometry Measurements

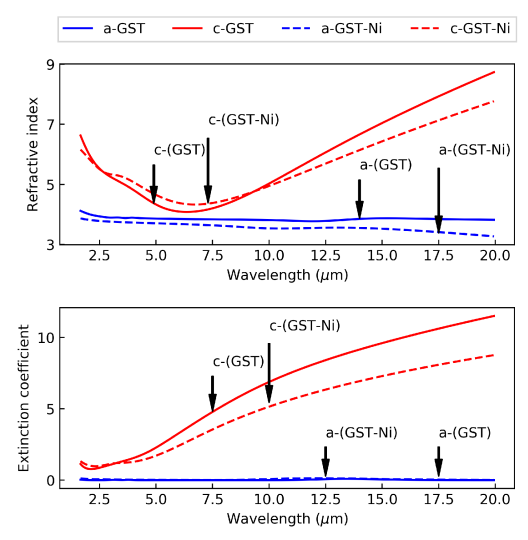


Figure 6: Real and imaginary parts of the complex refractive index vs wavelength for both amorphous and crystalline states of GST and GST-Ni.

The optical constants of the GST and GST-Ni at amorphous and crystalline states were obtained using ellipsometry. Figure 6 shows the behavior of refractive index and extinction coefficient of GST and GST-Ni as the phase switches. In undoped GST thin films, both the refractive index and extinction coefficient increase as

the structure changes from amorphous to fcc and then to the hcp state. The optical constants of Nickel-doped GST behaves similar to the undoped GST during the phase transition, which indicates that the nickel dopant inside the GST matrix does not affect the intrinsic optical properties of GST.

#### 4. CONCLUSIONS

In summary, nickel-doped GST thin films were prepared by magnetron co-sputtering of Ge<sub>2</sub>Sb<sub>2</sub>Te<sub>5</sub> and nickel targets. The nickel dopant could reduce the resistivity of GST in the amorphous state by 3 orders of magnitudes which enables a lower drive voltage for electrical switching from amorphous state to crystalline state. The XRD and Raman analysis confirm that the nickel dopant in GST matrix does not adversely affect the lattice structure and local structures. Ellipsometry results demonstrate that the optical dispersion of nickel-doped GST and undoped GST are essentially the same. The ability to maintain the optical properties while reduced the resistivity in the amorphous state gives the potential for GST-Ni to be utilized in high-speed electrically switchable phase modulators.

#### ACKNOWLEDGMENTS

This work is supported by the National Science Foundation under Grant No. 1710273 and the University of Dayton graduate school. The authors thank Rachel H. Rai from the Department of Chemical and Materials Engineering at the University of Dayton for the Raman measurements.

#### REFERENCES

- [1] Lombardo, D., Shah, P., Guo, P., and Sarangan, A., "Deep-uv interference lithography combined with masked contact lithography for pixel wiregrid patterns\textbf {~}," Bulletin of the American Physical Society 61 (2016).
- [2] Guo, P., Lombardo, D., and Sarangan, A., "Vanadium dioxide switchable components based on wiregrids for mid-infrared applications," in [Nanoengineering: Fabrication, Properties, Optics, and Devices XIV], 10354, 1035411, International Society for Optics and Photonics (2017).
- [3] Privitera, S., Rimini, E., and Zonca, R., "Amorphous-to-crystal transition of nitrogen- and oxygen-doped Ge 2Sb2Te5 films studied by in situ resistance measurements," *Applied Physics Letters* 85(15), 3044–3046 (2004).
- [4] Zhou, X., Xia, M., Rao, F., Wu, L., Li, X., Song, Z., Feng, S., and Sun, H., "Understanding Phase-Change Behaviors of Carbon-Doped Ge ¡sub¿2¡/sub¿ Sb ¡sub¿2¡/sub¿ Te ¡sub¿5¡/sub¿ for Phase-Change Memory Application," ACS Applied Materials & Interfaces 6, 14207–14214 (8 2014).
- [5] Privitera, S., Rimini, E., and Zonca, R., "Amorphous-to-crystal transition of nitrogen- and oxygen-doped Ge 2Sb2Te5 films studied by in situ resistance measurements," *Applied Physics Letters* **85**(15), 3044–3046 (2004).
- [6] Jeong, S.-M., Kim, K.-H., Choi, S.-M., and Lee, H.-L., "Influence of silicon doping on the properties of sputtered ge2sb2te5 thin film," *Japanese Journal of Applied Physics* 48(4R), 045503 (2009).
- [7] Wei, S., Li, J., Wu, X., Zhou, P., Wang, S., Zheng, Y., Chen, L., Gan, F., Zhang, X., and Li, G., "Phase characteristics of aluminum doped Ge\_2Sb\_2Te\_5 films prepared by magnetron sputtering," Optics Express 15(17), 10584 (2007).
- [8] Lie, C.-T., Kuo, P.-C., Hsu, W.-C., Wu, T.-H., Chen, P.-W., and Chen, S.-C., "Ge 2 Sb 2 Te 5 Thin Film Doped with Silver," *Japanese Journal of Applied Physics* 42(Part 1, No. 2B), 1026–1028 (2003).
- [9] Wei, S. J., Zhu, H. F., Chen, K., Xu, D., Li, J., Gan, F. X., Zhang, X., Xia, Y. J., and Li, G. H., "Phase change behavior in titanium-doped Ge2Sb2Te5 films," *Applied Physics Letters* **98**(23), 231910 (2011).
- [10] Guo, S., Hu, Z., Ji, X., Huang, T., Zhang, X., Wu, L., Song, Z., and Chu, J., "Temperature and concentration dependent crystallization behavior of Ge jsub¿2j/sub¿ Sb jsub¿2j/sub¿ Te jsub¿5j/sub¿ phase change films: tungsten doping effects," RSC Adv. 4(100), 57218–57222 (2014).
- [11] Zhu, Y., Zhang, Z., Song, S., Xie, H., Song, Z., Li, X., Shen, L., Li, L., Wu, L., and Liu, B., "Ni-doped gst materials for high speed phase change memory applications," *Materials Research Bulletin* **64**, 333–336 (2015).

- [12] Ding, K., Ren, K., Rao, F., Song, Z., Wu, L., Liu, B., and Feng, S., "Study on the Cu-doped Ge 2 Sb 2 Te 5 for low-power phase change memory," *Materials Letters* **125**, 143–146 (2014).
- [13] Kumar, S., Singh, D., Shandhu, S., and Thangaraj, R., "Chemical states and optical properties of thermally evaporated ge—te and ge—sb—te amorphous thin films," *Applied Surface Science* **258**(19), 7406–7411 (2012).
- [14] Morales-Sanchez, E., Prokhorov, E., Gonzalez-Hernandez, J., and Mendoza-Galvan, A., "Structural, electric and kinetic parameters of ternary alloys of gesbte," *Thin Solid Films* **471**(1-2), 243–247 (2005).
- [15] Guo, S., Hu, Z., Ji, X., Huang, T., Zhang, X., Wu, L., Song, Z., and Chu, J., "Temperature and concentration dependent crystallization behavior of ge 2 sb 2 te 5 phase change films: tungsten doping effects," RSC Advances 4(100), 57218–57222 (2014).
- [16] Němec, P., Nazabal, V., Moréac, A., Gutwirth, J., Beneš, L., and Frumar, M., "Amorphous and crystal-lized ge—sb—te thin films deposited by pulsed laser: Local structure using raman scattering spectroscopy," *Materials Chemistry and Physics* **136**(2-3), 935–941 (2012).
- [17] De Bastiani, R., Piro, A. M., Grimaldi, M. G., Rimini, E., Baratta, G. A., and Strazzulla, G., "Ion irradiation-induced local structural changes in amorphous thin film," *Citation: Appl. Phys. Lett* **92**, 241925 (2008).
- [18] Andrikopoulos, K., Yannopoulos, S., Kolobov, A., Fons, P., and Tominaga, J., "Raman scattering study of gete and ge2sb2te5 phase-change materials," *Journal of Physics and Chemistry of Solids* **68**(5-6), 1074–1078 (2007).
- [19] Li, T., Wu, L., Ji, X., Zheng, Y., Liu, G., Song, Z., Shi, J., Zhu, M., Song, S., and Feng, S., "Carbon doping induced ge local structure change in as-deposited ge2sb2te5 film by exafs and raman spectrum," *AIP Advances* 8(2), 025201 (2018).